

Behavior of concrete columns confined with both steel angles and spiral hoops under axial compression

Chunheng Zhou^{1a}, Zongping Chen^{*1,2}, Sheldon Q. Shi^{3,4b} and Liping Cai^{3c}

¹ College of Civil Engineering and Architecture, Guangxi University, 100 Daxue road, Nanning, China

² Key Laboratory of Disaster Prevention and Structure Safety of Chinese Ministry of Education, 100 Daxue road, Nanning, China

³ Department of Mechanical and Energy Engineering, University of North Texas, 3940 N. Elm – F101 P Denton, Texas, USA

⁴ School of Resources, Environment, and Materials, Guangxi University, Nanning, China

(Received November 29, 2017, Revised February 3, 2018, Accepted April 4, 2018)

Abstract. This study proposed a new type of concrete column that was confined with both steel angles and spiral hoops, named angle-steel and spiral confined concrete (ASCC) column. A total of 22 ASCC stub columns were tested under axial compression to investigate their behavior. For a comparison, three angle-steel reinforced concrete (ARC) stub columns were also tested. The test results indicated that ASCC column had a superior mechanical performance. The strength, ductility and energy absorption were considerably increased due to the improvement of confinement from spiral hoops. The confinement behavior and failure mechanism of ASCC column were investigated by the analysis of failure mode, load-deformation curve and section-strain distribution. Parametric studies were carried out to examine the influences of different parameters on the axial compression behavior of ASCC columns. A calculation approach was developed to predict the ultimate load carrying capacity of ASCC columns under axial compression. It was validated that the predicted results were in well agreement with the experimental results.

Keywords: ASCC column; axial compression; confinement; spiral; ultimate load carrying capacity; toughness

1. Introduction

In recent years, numerous studies were carried out on the behavior of steel reinforced concrete (SRC) columns, with many advances of its use in the construction of high-rise buildings and long-span structures. In the conventional steel reinforced concrete column, the steel section is always placed at the center of cross-section (Ky *et al.* 2015, Campian *et al.* 2015), in which the contribution of steel section to the flexural behavior of this column is limited (Hwang *et al.* 2016). Therefore, for better efficiency and economy, several studies (Xiao *et al.* 2017, Kim *et al.* 2013, Hwang *et al.* 2016, Campione 2011, Eom *et al.* 2013, Wang *et al.* 2015) focused on a SRC column with separate steel sections at the corners, such as angle-steel reinforced concrete (ARC) column, which was always square and rectangular cross-section, and four steel angles were placed at the corners of the cross-section and weld-connected with transverse reinforcing bars or battens. In this kind of column, the flexural capacity was increased under biaxial moments due to the corner-distribution of steel section (Hwang *et al.* 2016). A comparative study of traditional

SRC and ARC column eccentric axial load was conducted by Kim *et al.* (2013). Results showed that, when using steel angles at the corners, the flexural capacity was significantly increased. The ultimate moment capacity and flexural stiffness of ARC column were 1.44 and 1.48 times of those of the conventional SRC column with the same steel ratio, respectively. Furthermore, the corner steel angles and battens can provide confinement to the concrete core, improving the load-carrying capacity and ductility of the ARC column by placing the core concrete in the lateral stress (Hwang *et al.* 2016, Kim *et al.* 2013 and Campione 2011). Moreover, there are three other major advantages of ARC column. Firstly, the field rebar work can be reduced due to the prefabrication of steel sections (Hwang *et al.* 2016). Secondly, the longitudinal rebars of beams at the joints of RC beam and composite column can be conveniently placed, penetrating the joint without interruption by steel sections (Eom *et al.* 2013). Thirdly, the self-erectable steel cage can provide sufficient strength and rigidity to carry construction loads and remainder loads after the concrete is cured. Therefore, the amount of timber that is used to carry construction loads can be reduced. It is an effective way to save the cost of formwork and accelerate construction work (Hwang *et al.* 2016 and Wang *et al.* 2015).

Hence, several experimental and numerical studies on ARC column were conducted. An axial compression test on ARC specimen was performed by Hwang *et al.* (2016). The test results indicated that, under axial loading, the corner angles and the welded hoops provided adequate lateral

*Corresponding author, Professor,
E-mail: zpchen@gxu.edu.cn

^a Ph.D. Candidate, E-mail: chzhou2014@hotmail.com

^b Professor, E-mail: Sheldon.Shi@unt.edu

^c Professor, E-mail: Liping.Cai@unt.edu

confinement to the concrete to enhance the load-carrying capacity and deformation capacity. An experiment study on flexural strength and ductility of ARC specimen was carried out by Eom *et al.* (2013). Results showed that the flexural capacity of the ARC column was significantly greater than that of SRC columns with an H-section at the center of the cross-section and exhibited a more ductile behavior after the flexural yielding. Zheng and Ji (2008), Hwang *et al.* (2016) and Wang *et al.* (2015) performed a cyclic loading test and numerical analysis on ARC column, and compose beam-ARC column joint and frame of ARC column respectively. Results showed that they all owned good seismic performance. The hysteretic curves were relatively plump and there was no significant pinch phenomenon after the peak load. The deformation and energy dissipation capacities of the specimens were good and satisfied the requirements of the corresponding standard. The studies of existing RC columns strengthened with steel cage, have similar construction and working mechanism with ARC columns, suggesting their superior performance. It has been widely observed that this type of strengthening is fully effective for increasing the carrying capacity and ductility of RC columns due to the confinement pressures in the concrete core from steel angles and battens (Frangou *et al.* 1995, Adam *et al.* 2009, Garzón-Roca *et al.* 2011, Nagaprasad *et al.* 2009, Wu *et al.* 2006 and Campione 2012).

Although the ARC column exhibits superior feature and advantageous mechanical performance, there are still some disadvantages to limit its application. Firstly, the buckling of steel angles of ARC columns, both under static and dynamic loads, is observed in previous studies because of the insufficient lateral restraint. Therefore, the post-peak strength and ductility are significantly deteriorated since the confinement from steel angles is weakened (Hwang *et al.* 2016, Campione 2011 and Eom *et al.* 2014). In addition, the same as the other square confined concrete columns, such as reinforced concrete column and concrete-filled square steel tubular column, the effective lateral confining pressure from steel cage can only exert near the corners of section on ARC columns due to arching action (Montuori and Piluso 2009) (as show in Fig. 1(a)). Hence, the confined effectiveness of ARC columns would less than that of circular section columns such as the spiral confined concrete columns (Sheikh and Uzumeri 1980, Somes 1970, Cavaleri 2017). In order to increase the lateral confinement of the square confined concrete column, Ding *et al.* (2014), Yang *et al.* (2015) and Shih *et al.* (2013) used spiral hoops in the center of square concrete-filled steel tubular column and reinforced concrete column as the internal confinement,

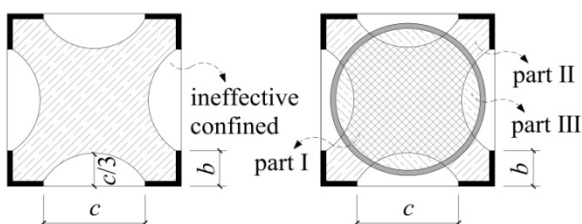


Fig. 1 Cross-sections of ARC column and ASCC column

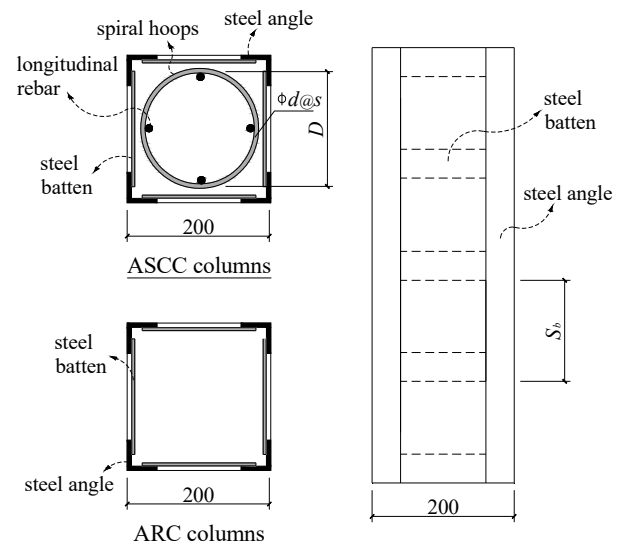


Fig. 2 Dimensions and details of specimens

which can provide double confinement to the core concrete. Results showed that the load-carrying capacity and ductility of this kind of columns can be improved significantly.

Therefore, considering the superior features of spiral reinforced concrete columns and the advantages of ARC columns, an angle-steel and spiral confined concrete (ASCC) column was developed in this study, aiming to addressing the aforementioned drawbacks of ARC column by placing a spiral hoop inside to strengthen the confinement on concrete (Fig. 1(b)). The ASCC column was expected to diminish the effect of the arching action in ARC column by using the spiral hoops and further support enough confinement when the steel angles buckling after the peak load. In this study, an experimental program was carried out to investigate the behavior and failure mechanism of ASCC columns under the pure compression. Afterwards, parametric analyses were carried out to investigate the influences of different parameters on the ultimate load carrying capacity, toughness and ductility of ASCC columns. Finally, a calculation approach was developed to predict the ultimate load carrying capacity of ASCC columns under the pure compression.

2. Experimental program

2.1 Test specimens

In this study, a total of 25 specimens were designed and fabricated for compression tests. The specimens included 22 ASCC stub columns and three ARC stub columns (Fig. 2), all with a square side length of 200 mm and a height of 600 mm. The geometric properties of the specimens are presented in Table 1.

For the specimens ASCC-1 to ASCC-3, different target strengths concretes (grade C30, C40 and C50, according to Chinese code GB 50010-2010) were used to investigate the multi-confinement effect of ASCC columns. In those specimens, four steel angles of L40×4 mm (width × flange thickness), steel battens of -40×4 mm (width × thickness)

Table 1 Design parameters and mechanical properties of specimens

NO.	C	Longitudinal rebar	Spiral hoops	D /mm	ρ_V /%	Steel angle /mm	ρ_A /%	Steel batten /mm	s_b /mm	ρ /%	N_u /kN	N_{u0} /kN	EA	μ
ASCC-1	C30	4 ϕ 10	ϕ 6@40	160	1.8	L40×4	3.1	-40×4	100	8.2	1754.5	451.0	162.6	4.46
ASCC-2	C40	4 ϕ 10	ϕ 6@40	160	1.8	L40×4	3.1	-40×4	100	8.2	2527.5	649.7	330.0	2.48
ASCC-3	C50	4 ϕ 10	ϕ 6@40	160	1.8	L40×4	3.1	-40×4	100	8.2	2803.0	720.6	336.0	1.39
ASCC-4	C30	4 ϕ 10	ϕ 6@20	160	3.5	L40×4	3.1	-40×4	100	8.8	2000.5	514.3	200.4	-
ASCC-5	C30	4 ϕ 10	ϕ 6@30	160	2.4	L40×4	3.1	-40×4	100	8.3	1847.0	474.8	195.0	5.59
ASCC-6	C30	4 ϕ 10	ϕ 6@50	160	1.4	L40×4	3.1	-40×4	100	7.8	1721.5	442.5	162.0	3.74
ASCC-7	C30	4 ϕ 10	ϕ 6@60	160	1.2	L40×4	3.1	-40×4	100	7.7	1567.5	403.0	162.6	3.86
ASCC-8	C30	4 ϕ 10	ϕ 6@80	160	0.9	L40×4	3.1	-40×4	100	7.5	1480.5	380.6	166.2	3.53
ASCC-9	C30	4 ϕ 10	ϕ 6@100	160	0.7	L40×4	3.1	-40×4	100	7.4	1458.5	374.9	159.0	2.78
ASCC-10	C30	4 ϕ 10	ϕ 8@70	160	1.8	L40×4	3.1	-40×4	100	8.0	1661.0	427.0	163.8	3.82
ASCC-11	C30	4 ϕ 10	ϕ 10@115	160	1.8	L40×4	3.1	-40×4	100	8.0	1396.5	359.0	159.0	3.10
ASCC-12	C30	4 ϕ 10	ϕ 6@40	160	1.8	L50×4	3.9	-40×4	100	8.8	1911.5	491.4	288.0	4.45
ASCC-13	C30	4 ϕ 10	ϕ 6@40	160	1.8	L30×4	2.3	-40×4	100	7.2	1556.5	400.1	126.6	3.79
ASCC-14	C30	4 ϕ 10	ϕ 6@40	160	1.8	L40×4	3.1	-40×4	80	9.8	1848.0	475.1	169.2	3.90
ASCC-15	C30	4 ϕ 10	ϕ 6@40	160	1.8	L40×4	3.1	-40×4	120	7.4	1725.0	443.4	139.2	4.10
ASCC-16	C30	4 ϕ 10	ϕ 6@40	160	1.8	L40×4	3.1	-40×4	140	7.0	1679.0	431.6	145.2	3.74
ASCC-17	C30	4 ϕ 10	ϕ 6@40	160	1.8	L40×4	3.1	-40×4	160	6.8	1602.5	412.0	144.0	3.80
ASCC-18	C30	4 ϕ 12	ϕ 6@40	160	1.8	L40×4	3.1	-40×4	100	8.5	1778.0	423.3	174.0	4.81
ASCC-19	C30	6 ϕ 10	ϕ 6@40	160	1.8	L40×4	3.1	-40×4	100	8.4	1899.5	443.8	210.0	5.06
ASCC-20	C30	4 ϕ 10	ϕ 6@40	180	1.6	L40×4	3.1	-40×4	100	8.1	1857.5	478.1	165.6	4.31
ASCC-21	C30	4 ϕ 10	ϕ 6@40	140	2.0	L40×4	3.1	-40×4	100	7.9	1565.5	403.0	202.8	5.42
ASCC-22	C30	4 ϕ 10	ϕ 6@40	120	2.4	L40×4	3.1	-40×4	100	7.7	1546.0	397.9	213.6	5.93
ARC-1	C50	—	—	—	—	L40×4	3.1	-40×4	100	6.3	2202.5	710.5	300.0	1.16
ARC-2	C30	—	—	—	—	L40×4	3.1	-40×4	100	6.3	1130.5	364.7	160.6	4.10
ARC-3	C30	—	—	—	—	L40×4	3.1	-40×4	140	5.4	1035.0	333.9	146.0	3.10

* Note: C = Concrete strength grade; D = diameter of spiral between bar centers; ρ_V = ratio of volume of spiral reinforcement to total volume of core confined by the spiral; ρ_A = ratio of steel angle to cross-section; s_b = spacing of steel battens; ρ = total of steel ratio; N_u = experimental axial load carrying capacity of specimens; N_{u0} = The experimental axial load carrying capacity of the column divide by the corresponding steel ratio; EA = Axial compression stiffness of specimens; μ = ductility of specimens, specific definition was given in the Section 3.4

with a spacing of 100 mm, four B10 longitudinal bars and A6 spiral hoops with the spacing of 40 mm were used. For the specimens ASCC-4 to ASCC-9, different pitches of spiral hoops were considered to study the confinement effect of volumetric ratio of steel spiral on the load carrying capacity and ductility. In the specimens ASCC-10 and ASCC-11, different diameters of hoops with a uniform volumetric ratio (the same as that of ASCC-1 equaling to 1.8%) were used. For the specimens ASCC-12 and ASCC-13, different steel ratios of angles were considered to investigate the influence on the mechanical behavior caused by the steel ratio. In these specimens, steel angles of L50×4 mm and L30×4 mm were used. For the specimens ASCC-14 to ASCC-17, the influence of volumetric ratio of steel batten on the constraint effect caused by variation of batten spacing was investigated. The batten spacings in those specimens were 80 mm, 120 mm, 140 mm and 160 mm, respectively. For the specimens ASCC-18 and ASCC-19,

the longitudinal bars of four B12 and six B10 with a same reinforcement ratio equal to 1.1% were used to investigate the effect of configuration way of longitudinal bars on the strength and stiffness. In the specimens ASCC-20 to ASCC-22, different confined core diameters, as determined by diameter of spiral, were considered to investigate the effect of confined area size on the mechanical behavior of ASCC column. In these columns, the diameter of spiral hoops was 180 mm, 140 mm and 120 mm, respectively. Specimens ARC-1 to ARC-3 are conventional angle reinforced concrete column without confinement of spiral hoops inside. Different concrete strengths and spacings of batten were considered in these specimens. The steel configuration and concrete strength of specimens ARC-1, ARC-2 and ARC-3 were the same as those of specimens ASCC-3, ASCC-1 and ASCC-16, respectively.

In all specimens, the four angles were placed at the corners of the cross-section. Steel battens joined to the



Fig. 3 Steel and reinforcing cages after construction

Table 2 Mechanical properties of steel

Bar and shape steel	Yield stress f_y /MPa	Ultimate stress f_u /MPa	Elastic modulus E_s / $\times 10^5$ MPa	Yield strain ϵ_y / $\mu\epsilon$	Elongation /%
$\phi 6$	405	595	2.11	1967	—
$\phi 8$	387	588	2.10	1833	—
$\phi 10$	375	543	2.08	2300	25.63
$\phi 10$	401	608	1.97	2190	25.32
$\phi 12$	418	642	1.90	2293	22.50
-30 \times 4	450	639	2.27	2073	24.17
-40 \times 4	275	361	2.09	1583	31.88
-50 \times 4	519	734	2.25	2327	15.00
L30 \times 4	474	644	2.09	2403	18.33
L40 \times 4	539	765	2.02	2640	17.50
L50 \times 4	478	693	1.97	2593	21.25

*Note: The elongation of A6 and A8 bars cannot be obtained in this test due to the small diameter

inside surface of steel angles by groove welding with various spacings. All steel cages in the specimens were fabricated. For ASCC specimens, longitudinal bars and spiral hoops were bound to make a reinforcing cage. The formed reinforcing cage was then placed in the center of the steel part as the internal confinement. The steel part and reinforcing cage after construction can be seen in Fig. 3.

2.2 Materials

The longitudinal and spiral reinforcement that used in this study are deformed bars and plain bars respectively specified in Chinese code GB 50010-2010. Steel angles and steel plates classified as Q235 were used according to the Chinese code GB/T 700-2006. Standard coupons were prepared from each type of steel and reinforcement and tested under uniaxial tension and the results are summarized in Table 2.

For each concrete mixture, three concrete cubes with a dimension of 150 mm \times 150 mm \times 150 mm were tested for cubic compressive strength f_{cu} in accordance with the Chinese code GB/T 50081-2002. The average 28-day cube strengths of C30, C40 and C50 concretes were equal to 28.3 MPa, 43.4 MPa and 52.2 MPa corresponding to prism compressive strength of 18.2 MPa, 29.0 MPa and 34.9 MPa,

respectively, which were obtained according to the Chinese code GB 50010-2010. The column specimens were tested starting at 90 days after the concrete casting. The 90-day corresponding prism compressive strengths of specimens were estimated according to Eq. (1) specified in ACI209R-08. For C30, C40 and C50 concretes, the compressive strengths with 90-day were equal to 20.4 MPa, 32.5 MPa and 39.1 MPa, respectively, which can be easily obtained.

$$f_{ct} = \left(\frac{t}{4.0 + 0.85t} \right) f_{c28} \quad (1)$$

Where f_{ct} is concrete compressive strength at any time t , MPa; t is time from concrete casting, days; f_{c28} is concrete mean compressive strength at 28 days, MPa.

2.3 Test setup and instrumentation

Fig. 4 shows the test setup and instrumentation for the column specimens. The axial load was applied to the specimens by a 10000 kN servo testing machine. All specimens were tested using a displacement control mode with a loading rate of 2 mm/min, until the dropped load reached around 70% of its ultimate load. In order to reduce

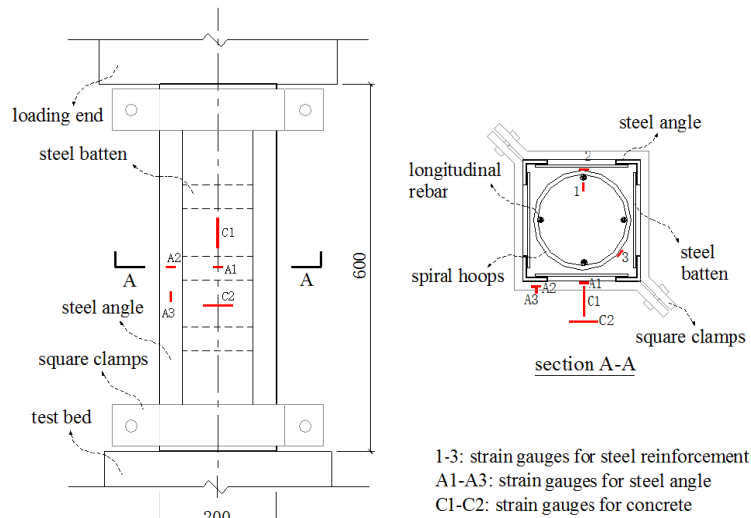


Fig. 4 Test setup and instrumentation



(a) Specimen ARC-2



(b) Specimen ASCC-1



(c) Specimen ASCC-17

Fig. 5 Failure mode of specimens

the effect of test result due to looseness of both ends, each specimen was preloaded with 50 kN before start of the actual loading. The axial load and deformation during the loading process were recorded by a data logger automatically. Two square clamps (Fig. 4) were contracted to confine the end regions of specimens to avoid unexpected failure.

A series of strain gauges were located mid-height of specimens, as shown in Fig. 4, to measure the compressive and tensile strains at the cross-section. Each specimen was instrumented with three gauges placed on the reinforcing bars (1-3), three gauges placed on the steel angles and battens (A1-A3) and two gauges placed on the concrete of specimen surface (C1-C2). The strains were acquired using a DH3818 static strain measurement system.

3. Results and discussion

3.1 Failure modes

Fig. 5 shows the representative failure modes of ARC stub columns and ASCC stub columns. All columns start

failing with cracking of concrete. Tiny cracks were formed and then propagated, which can be noted at the surface of ineffective confined concrete when the load reached to about 70% of the ultimate load. And then the extension of cracks was restricted due to the confinement of transversal steel battens, although the amount of them increased. When columns were loaded to 80% of the ultimate load, the concrete spalling was initiated and followed by the buckling of steel angles. Nevertheless, columns still exhibited a good deformability after the peak load. Because of the additional amount of lateral confinement provided by spiral hoops, the concrete spalling in the ARC columns was much less serious in the ASCC columns at the ultimate load. In the ASCC columns with a large spacing of steel battens, a further crushing and spalling of concrete can be observed in Fig. 5(c).

3.2 Axial load-deformation response

The axial load-deformation curves of all specimens are presented in Fig. 6 and compared by different parameters. All columns showed elastic behavior at the initial stage, indicated by a linear increase in axial load with an increase

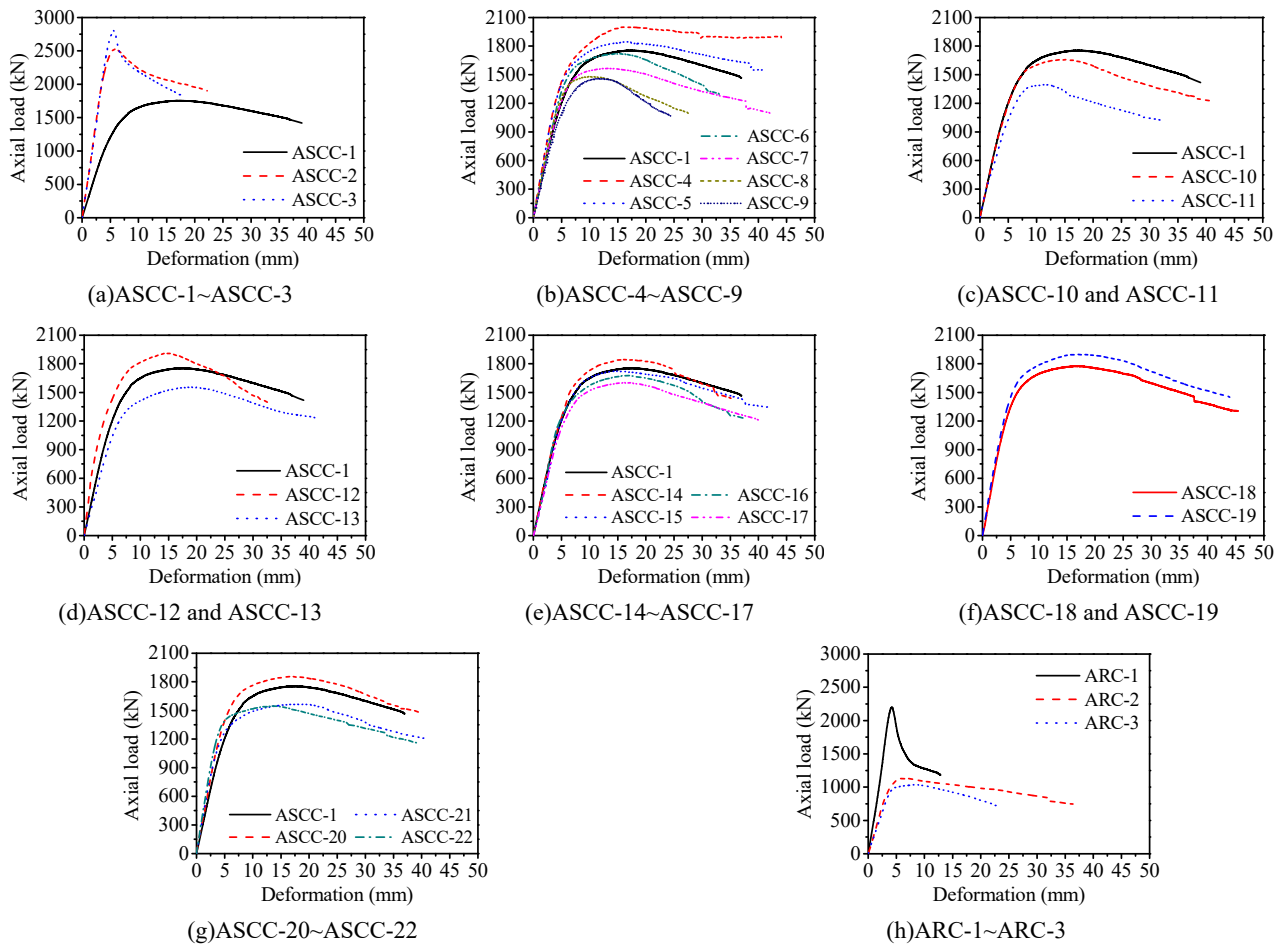


Fig. 6 Axial load-deformation curves

in the deformation of axial load-deformation curves. The curves began to exhibit nonlinear behavior when the axial load reached about 70% of the ultimate load. The ascending sections of all curves were similar while the descending sections of those were varied.

In Fig. 6 and Table 1, the axial load carrying capacity of ASCC columns was 27.3%-62.2% higher than that of ARC columns due to the improvement of confinement from internal spiral hoops. In order to consider the cost of steel, the load carrying capacities were normalized by the ratio of steel (The normalized load carrying capacity N_{u0} equals to the measured load carrying capacity of the column divide by the corresponding steel ratio). The normalized load carrying capacity N_{u0} of each specimen is showed in Table 1. It can be seen that the normalized load carrying capacity of ASCC columns was 2.8%-41.0% higher than that of the ARC column.

Figs. 6(a) and (h) show the axial load-deformation responses with different concrete strengths. It is observed that, for both the ASCC columns and ARC columns, the peak loads of specimens with higher strengths of concrete were higher than those with lower strengths of concrete. Nevertheless, the strength declined after the peak load in the later was more gradual in the former. It can be also observed that a rapid decline of load carrying capacity in the load-deformation curves of specimens ASCC-2, ASCC-3 and ARC-1. It is because the smaller ductility of C50

concrete was used in these specimens.

In Fig. 6(b), the axial load-deformation responses with different spiral pitches are compared. It can be seen that the larger pitch of spiral hoops, the more flat of descending part in their axial load-deformation curves of specimens. It was also worth to mention that a suddenly load drop occurred in the descending sections in some curves (ASCC-5, ASCC-7, ASCC-14 and ASCC-16 etc.) due to the rupture of steel angles and batten.

Fig. 6(c) shows the axial load-deformation responses with different hoop-diameters. In the figure, the larger the hoop-diameter the higher peak load and more flat the descending part of the curves can be seen.

Fig. 6(d) shows the axial load-deformation responses with different angle-steel ratios. It can be seen that, with the increase of angle-steel ratio, the peak load increased and the rising part of curves was steeper.

In Fig. 6(e), the axial load-deformation responses with different batten spacings are compared. It is similar to the effect of spiral pitch that the larger batten spacing, the more flat of descending part and the fuller of the axial load-deformation curves.

Fig. 6(f) shows the axial load-deformation responses with different configuration way of longitudinal bars. It is observed that, the peak load of specimens ASCC-19 with six B10 was higher than that of ASCC-18 with four B12.

In Fig. 6(g), the axial load-deformation curves with

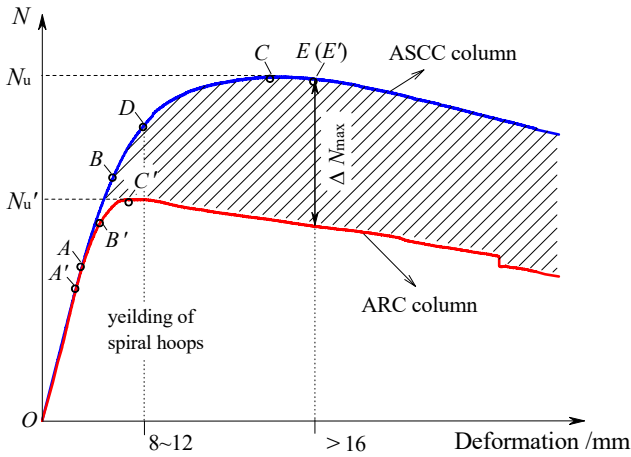


Fig. 7 Typical axial load-deformation behavior of ASCC column and ARC column

different confined core diameter. The peak load increased gradually with the increase of the confined core diameter. But the descending part was steeper in the curve of specimen with larger confined core diameter.

Fig. 7 shows a comparison of typical axial load-deformation behaviors for ASCC column and ARC column. Point A-E, A'-E' indicate the main events in the behavior of ASCC column and ARC column respectively. At points A and A', the concrete crack was firstly observed on the specimens. At points B and B', the concrete spalling occurred at the ineffective confined concrete. At points C

and C', specimens loaded to the peak load. At point D, the strain of spiral hoops in ASCC column reached yield strain. In the case of point E (E'), it was indicated the maximum difference of load between ASCC column and ARC column. In the early stage of loading, the curvatures of ascending sections were similar while the load of ASCC column was increased faster than that of ARC with the increase of deformation after the cracking of concrete. The concrete spalling of the ASCC column was initiated later than those of ARC column. Compared to the ARC column, much higher peak load, more sufficient deformation and more significant energy absorption (the difference as indicated by the shade area between load-deformation curves of ASCC column and ARC column) of ASCC column can be seen in Fig. 7, due to the offset of arching action by inner spiral hoops. The difference of load and energy absorption increased as the increase in deformation after the yielding of spiral hoops up to point E.

3.3 Axial load-strain response and strain distribution

Fig. 8 shows the typical load-strain curves obtained from reinforcing bars, steel angles, steel batten and concrete in the specimens. It can be noticed that the strain of spiral hoops increased faster than that of steel batten in ASCC columns, indicating that the lateral confinement provided by spiral reinforcement was more significant than that provided by steel batten. Figs. 8(a)-(c) shows that the strains of all longitudinal bars, spiral hoops, steel angles and

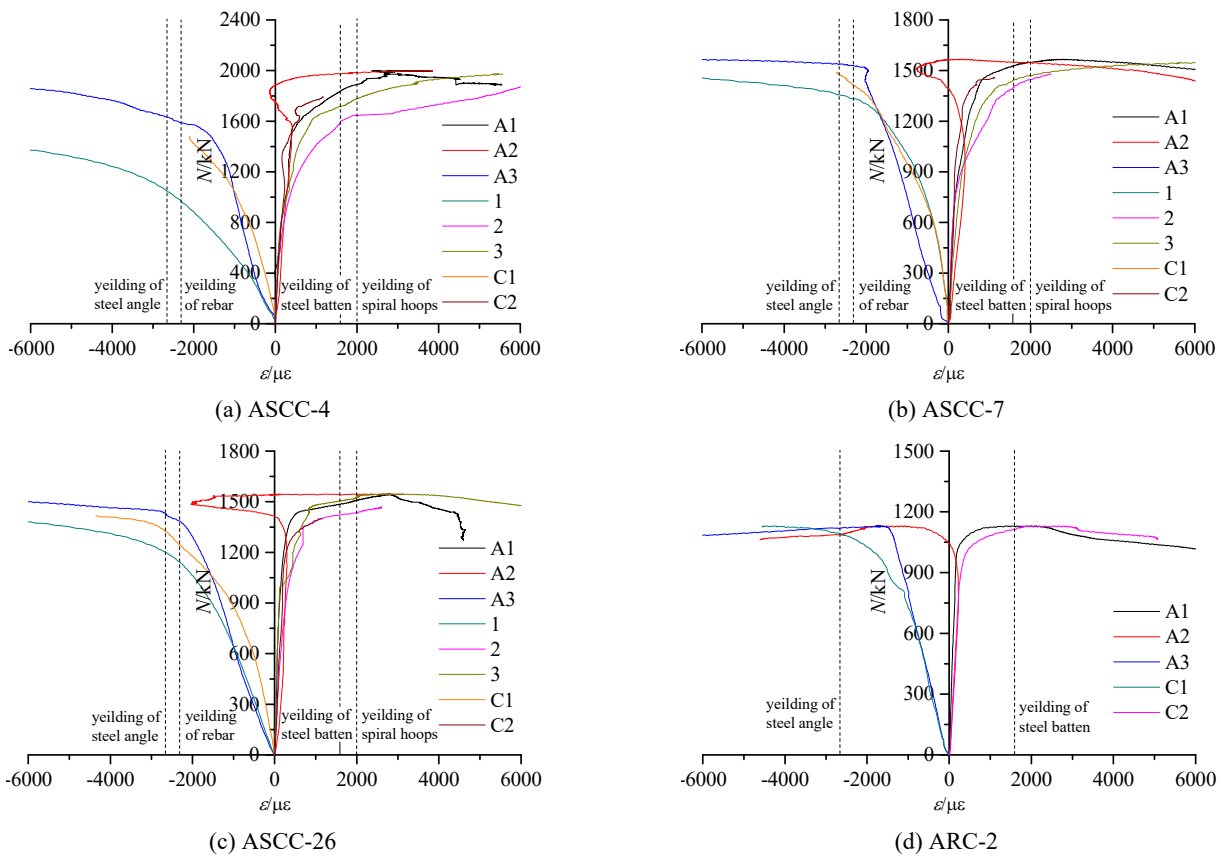


Fig. 8 Axial load-strain curves

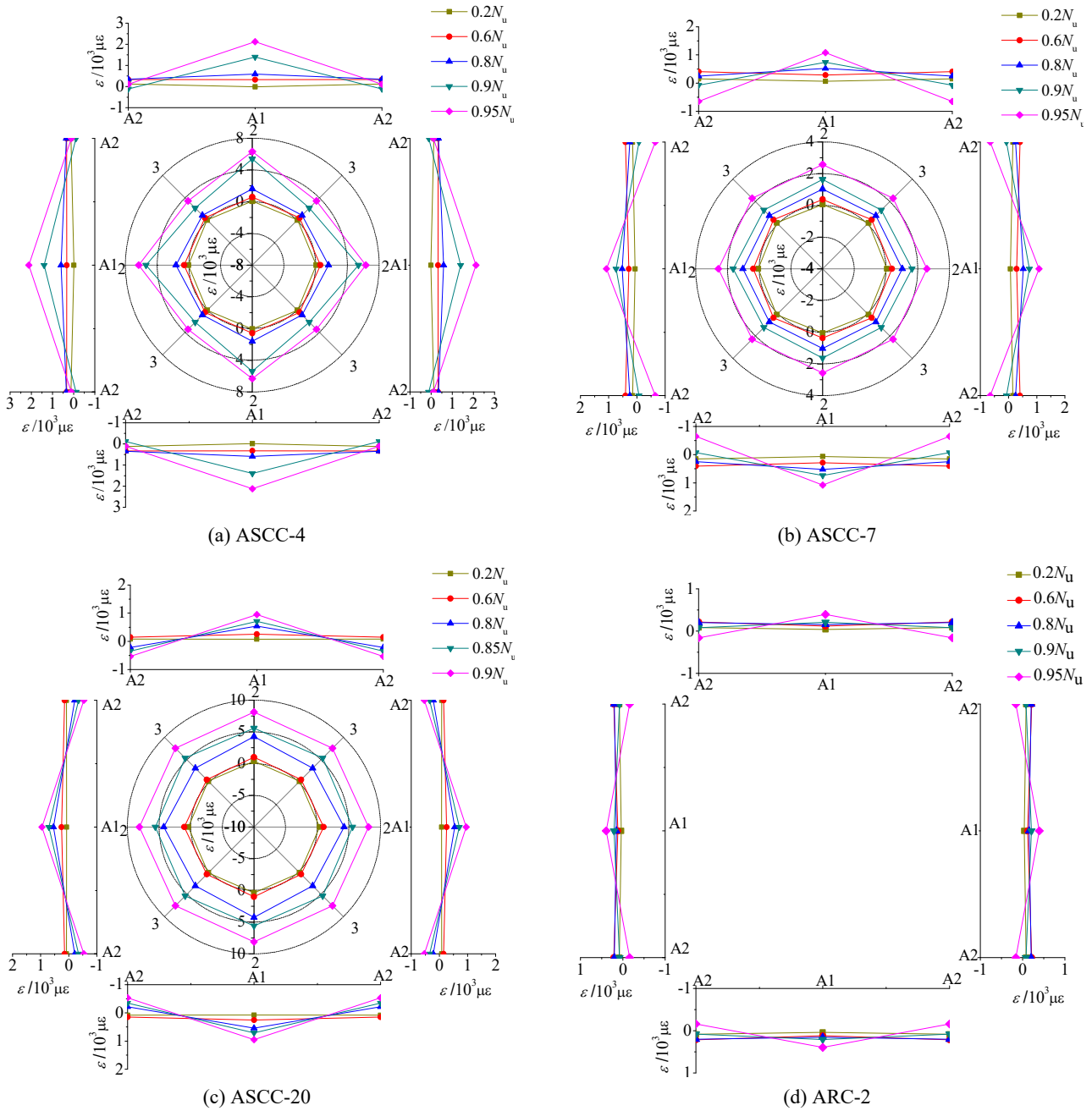


Fig. 9 Strain distribution of cross-section

battens reached the yield strain before peak in ASCC columns. In the case of ARC columns, the steel angles yield before the load reached to the ultimate load while the stress of steel batten was smaller than the yield stress as shown in Fig. 8(d). It was indicated that the steel batten can't be fully developed in ARC columns while all material strengths fully played their roles in ASCC columns under the axial load.

Because of symmetry, the typical cross-section strain distribution of columns can be obtained by gauges 2, 3, A1 and A2 placing in spiral hoops and steel battens as shown in Fig. 9. It is worth noting that the strain for the steel battens was measured in the horizontal direction. The strain for the spiral hoops was measured with an angle to the horizontal direction due to the inclined direction of spiral. However, the

inclined angle of the spiral is very small. Therefore, the direction of strain of spiral hoops was considered approximately the same as that of the steel battens (of horizontal direction) in this study. In Fig. 9, the lines showing round distribution in the center represent the strain distribution of spiral hoops. Similarly, the lines in the four sides mean the strain distribution of steel batten and angle. It can be seen that all strains were very small regardless of spiral hoops and steel battens, and distributed uniformly before the load reached 80% of the ultimate load. Whereas, the strain distribution in spiral hoops and steel battens exhibited a non-uniform phenomenon when the load was greater than 80% of the ultimate load in specimens. At this time, strains in the parts of spiral hoops and the steel battens away from the corners were larger than those near the

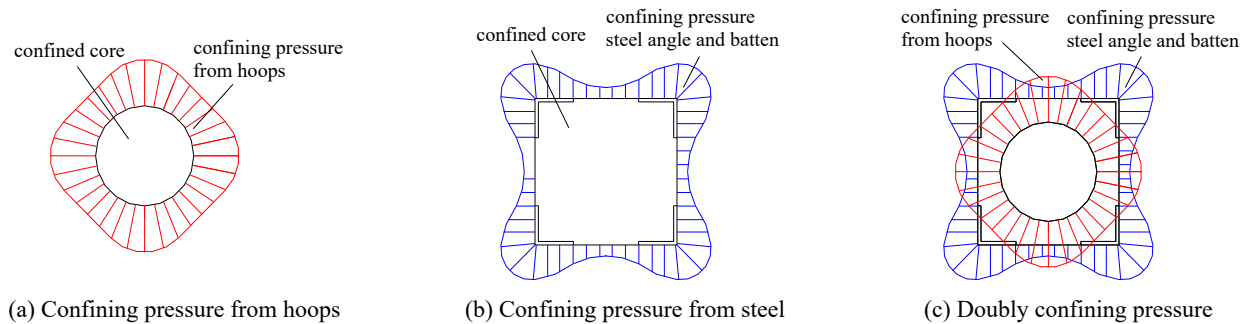


Fig. 10 Distribution of confining pressure in cross-section

section corners. It was indicated that the confining pressure, which dominated by stress of spiral hoops, on the part of concrete core away from the corners were larger than those near the corners, as illustrated in Fig. 10(a). Nevertheless, the confining pressure from steel angles and battens can be exerted effectively on the part of concrete only near the section corners, as shown in Fig. 10(b), due to the arching action.

3.4 Parametric analysis

An influence analysis of various parameters on mechanical properties of ASCC, including the ultimate load carrying capacity, stiffness and ductility, which were obtained from experimental results, were conducted and are summarized in Table 1. The ductility μ was defined as (Kim *et al.* 2013)

$$\mu = \Delta_u / \Delta_e, \quad (2)$$

where Δ_u is the ultimate deformation correspond to 80% of N_u at the descending section, and Δ_e is the deformation when initial steel yielding or concrete crushing occurred.

3.4.1 Effect of concrete strength

The specimens ASCC-1, ASCC-2 and ASCC-3 with concrete strengths of 30 MPa, 40 MPa and 50 MPa, respectively, were used to investigate the influence of concrete strength. In Table 1 and Fig. 6(a), it can be seen that, with an increase in concrete strength both ultimate load carrying capacity and toughness, the ductility was decreased, the same as other concrete columns. When the concrete strength increased from 30 MPa to 50 MPa, the decrease of ductility of the ASCC column was 68.8%, which less than that of the ARC column of 71.7%. It was suggested that the ASCC column with spiral hoops inside can reduce the decline of ductility in column with the increase of concrete strength.

3.4.2 Effect of spiral pitch

The ASCC-1 and ASCC-4 to ASCC-9 were detailed with varied spiral pitches ranging from 20 mm to 100 mm to investigate the influence of spiral pitch on mechanical properties. In Table 1 and Fig. 6(b), it is shown that the ultimate load carrying capacity and ductility are linearly improved by reducing the spiral pitch, i.e., increasing the amount of confinement through the improvement of

volumetric ratio of the ties brings on improved ultimate load carrying capacity and ductility. Especially in the specimen ASCC-4, there was almost no evident strength degradation after the peak load. When the volumetric ratio of the ties doubly increased from 1.2% in ASCC-7 to 2.4% in ASCC-5, the ultimate load carrying capacity and ductility were increased by 17.8% and 44.8% respectively. However, the toughness was shown an increase when the spiral pitch decreased from 40 mm to 20 mm, while almost no improvement was found when it decreased from 100 mm to 40 mm.

3.4.3 Effect of hoop-diameter

Table 1 and Fig. 6(c) show the influence of hoop-diameter on mechanical properties by comparing the specimens ASCC-1, ASCC-10 and ASCC-11, in which they had a same volumetric ratio of the ties, but different diameters of spiral hoops. When the diameter of hoops increased from 6 mm to 10 mm with a uniform volumetric ratio, there was a significant increase in ultimate load carrying capacity and ductility and only a slight increase in toughness, indicating that the smaller diameter of hoops with a same volumetric ratio was needed for ASCC column to obtain superior mechanical properties.

3.4.4 Effect of steel ratio

In Table 1 and Fig. 6(d), the effect of steel ratio was compared using the specimens of ASCC-1 (3.1% of steel ratio), ASCC-12 (3.9% of steel ratio) and ASCC-13 (2.3% of steel ratio). ASCC-1 and ASCC-12 show ductility gains of 12.1% and 12.3% in comparison with ASCC-13. However, the effect of the increase of steel ratio was more significant on the ultimate load carrying capacity and toughness, showing increases of 12.7% and 28.4% in ASCC-1, and improvements of 22.8% and 127.5% in ASCC-12 compared to ASCC-13.

3.4.5 Effect of batten spacing

ASCC-1 and ASCC-14 to ASCC-17 were detailed with batten spacings varied from 80 mm to 160 mm to investigate the influence on mechanical properties, as shown in Table 1 and Fig. 6(e). The ultimate load carrying capacity and ductility were increased with the decrease of spacing batten. The ductility in ASCC-14 was experienced a sudden load drop after the peak load due to the rupture of steel batten. It was exhibited an improvement of the ultimate load carrying capacity and ductility since the

amount of confinement increased by means of the improvement of volumetric ratio of steel batten. When the volumetric ratio of steel batten doubly increased from 2% in ASCC-15 to 4% in ASCC-14, the ultimate load carrying capacity was increased by 7.1%. Compared with the effect of spiral pitch, it was indicated that the increase of volumetric ratio of steel batten was less effective in enhancement of ultimate load carrying capacity for ASCC columns. The toughness showed an increase in the specimens with smaller batten spacing and no improvement in that with larger batten spacing, when the spacing of batten decreased, which was similar to the effect of spiral pitch.

3.4.6 Effect of configuration way of longitudinal bars

Table 1 and Fig. 6(f) show the influence of configuration way for longitudinal bars of four B12 and six B10 with a same reinforcement ratio. It can be seen that the ultimate load carrying capacity, toughness and ductility of the ASCC-19 with six B10 was 6.8%, 20.7% and 5.2% higher than those of the ASCC-18 with four B12. It was suggested that the smaller diameter of longitudinal bar should be used in the ASCC column with the same reinforcement ratio.

3.4.7 Effect of confined core diameter

Table 1 and Fig. 6(g) show that the ultimate load carrying capacity was increased with the increase of confined core diameter. However, the toughness and ductility showed a decrease when the diameter of confined core increased.

4. Axial load carrying capacity calculation

The adopted theoretical concrete model was proposed by Mander *et al.* (1988), in which the ineffective confined by arching action can be considered, as follows

$$\sigma_{cc} = \frac{f_{cc} x r}{r - 1 + x^r} \quad (3)$$

where σ_{cc} is compressive concrete stress; f_{cc} is compressive strength of confined concrete, MPa.

$$x = \frac{\varepsilon_c}{\varepsilon_{cc}} \quad (4)$$

$$\varepsilon_{cc} = \varepsilon_{c0} \left[1 + 5 \left(\frac{f_{cc}}{f_{c0}} - 1 \right) \right] \quad (5)$$

where ε_c is compressive concrete strain; ε_{cc} is compressive strain of confined concrete; f_{c0} is compressive strength of unconfined concrete, MPa; and ε_{c0} is the corresponding strain.

$$r = \frac{E_c}{E_c - E_{sec}} \quad (6)$$

$$E_c = 5000 \sqrt{f_{c0}} \quad (7)$$

$$E_{sec} = \frac{f_{cc}}{\varepsilon_{cc}} \quad (8)$$

where E_c and E_{sec} are the tangent and secant elastic models of concrete

For confined concrete compressive strength f_{cc} , a “five-parameter” constitutive model is used and given as follow

$$f_{cc} = f_{c0} \left(-1.254 + 2.254 \sqrt{1 + \frac{7.94 f_1}{f_{c0}}} - 2 \frac{f_1}{f_{c0}} \right) \quad (9)$$

where f_1 is lateral confining pressure, MPa.

According to force balance analysis (Fig. 11), the lateral confining pressure from spiral hoops is given by

$$f_1 = 0.5 k_e \rho_v f_{ys} \quad (10)$$

$$k_e = \frac{1 - \frac{s'}{2D}}{1 - \rho_{cc}} \quad (11)$$

Similarly it can be shown that from steel batten in the x and y directions

$$f_{lx} = k_e \rho_x f_{yb} \quad (12)$$

$$f_{ly} = k_e \rho_y f_{yb} \quad (13)$$

$$k_e = \frac{\left[1 - 0.67 \left(1 - \frac{2b}{a} \right) \right] \left(1 - \frac{s'_b}{2a} \right)^2}{1 - \rho_{cc}} \quad (14)$$

where k_e is confinement effectiveness coefficient; ρ_v is volumetric ratio of spiral hoops to confined concrete; ρ_x and ρ_y are, respectively, the volumetric ratio of steel batten in x and y direction; f_{ys} and f_{yb} are tensile strength of spiral hoops and steel batten respectively, MPa; s' and s'_b are clear vertical spacing of spiral and that of steel batten, mm; ρ_{cc} is ratio of area of longitudinal bars to the area of concrete core section; a is length of cross-section; b is side length of steel angle, mm.

In order to predict the load carrying capacity, the concrete in the cross-section of ASCC column is divided into three parts by means of their different confinement levels, as shown in Fig. 1. The concrete in part I inside the

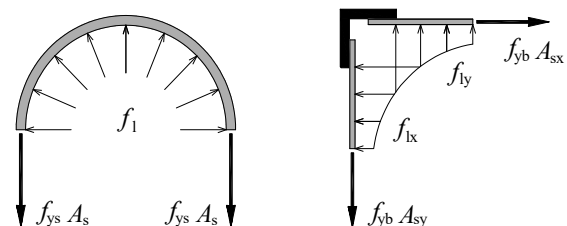


Fig. 11 Analysis of lateral pressure

spiral hoops is doubly confined by spiral hoops and steel section. The concrete in part II between spiral hoops and steel angles is singly confined by steel section. In the case of the concrete in part III, which is also inside the spiral hoops, is singly confined by spiral hoops due to the arching action.

Different constitutive laws have been adopted in various parts depending on their actual confinement by the actions of spiral hoops and steel cage. For the concrete confined by spiral hoops in part III, its constitutive relation and confined compressive strength f_{cIII} can be predicted using Eqs. (3)-(11). For the concrete confined by steel angles and battens in part II, the prediction of its constitutive relation and confined compressive strength f_{cII} can be performed using Eqs. (3)-(8) and Eqs. (12)-(14) and the diagram is depicted in Fig. 12, in which the arching action is considered in a rectangular section (Mander *et al.* 1988). In Fig. 12, the vertical axis means the maximum of f_{lx} and f_{ly} , the bottom of the horizontal axis means the minimum of f_{lx} and f_{ly} , and the top of the horizontal axis means f_{lx}/f_{ly} . For the doubly confined concrete in part I, Eqs. (3)-(11) can still be adapted to predict compressive strength f_{cI} by replacing f_{cII} with f_{c0} to evaluate the constitutive relation and confined compressive strength because the concrete doubly confined by spiral hoops in the strengthened section by the single-confining of steel section that is, substantially, the same confined by spiral hoops in the unconfined concrete. The different constitutive relationships for three parts of confined concrete with reference to specimen ASCC-1 are

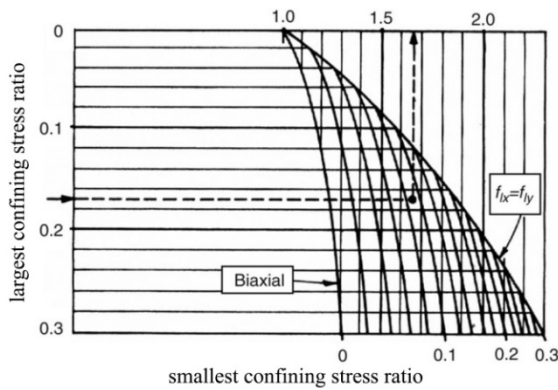


Fig. 12 Confined strength determination for rectangular sections

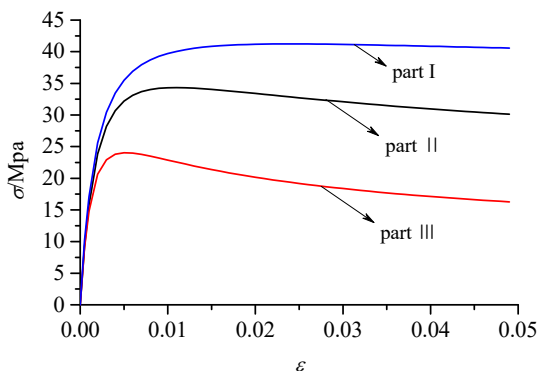


Fig. 13 Concrete constitutive relation for different parts

shown in Fig. 13.

The strength of the section of steel angles is predicted according to the Chinese Code GB50017, in which the buckling is considered by a stability coefficient, as follow

$$N_A = \varphi f_{ya}' A_{sa} \tag{15}$$

where φ is the stability coefficient; f_{ya}' is yielding strength of steel angle, MPa; A_{sa} is aggregate cross-sectional area of steel angles, mm^2 .

Since no buckling occurred in the longitudinal bars, the ultimate strength of the section of longitudinal bars is predicted as follows

$$N_s = f_y' A_s \tag{16}$$

where f_y' is yielding strength of longitudinal bar, MPa; A_s is aggregate cross-sectional area of longitudinal bar, mm^2 .

According to the superposition principle, the axial load carrying capacity of ASCC can be predicted as follows

$$N = f_{cI}A_I + f_{cII}A_{II} + f_{cIII}A_{III} + N_A + N_s \tag{17}$$

where A_I , A_{II} and A_{III} are the cross-sectional area of the part I, part II and part III, respectively, mm^2 .

In Table 3, the experimental results of load carrying capacity N_u were compared with the predicted results of load carrying capacity N_p by Eq. (17). The average ratio of N_u to N_p is 0.968 with a variance of 0.008. Therefore, the results of the proposed formula are satisfactory agreement with experimental results.

5. Conclusions

To investigate the axial compressive behavior of ASCC columns, 22 ASCC stub columns and three ARC stub columns were fabricated and tested in this study. The confining behavior and failure mechanism was explored by the analysis of the failure mode, load-deformation response and section strain distribution of specimens. The tests also examined the parametric influence of SRCC column detailing on ultimate load carrying capacity, toughness and ductility. The test results of ultimate load carrying capacity were compared with predictions, and the following conclusions can be drawn:

- The failure mode of ASCC columns under axial compression was similar to that of ARC columns. However, due to the confinement effect of spiral hoops, the concrete spalling in the ARC columns is much less serious in the ASCC columns at the ultimate load. The larger the spacing of steel battens, the more damage of ASCC columns.
- Using spiral hoops in ARC column to amplify the confining effect on concrete by offsetting the arching action could significantly improve the peak load and after peak behavior. In comparison to the ARC column, ASCC column shows a more sufficient deformation and energy absorption.

- All reinforcement and steel yield before the peak loads of ASCC columns were reached, and showed a non-uniform distribution in the cross-section, indicating a non-uniform distribution of the confining pressure. The lateral confinement provided by the spiral reinforcement plays a more significant role than that provided by steel batten. The confining pressure provided by spiral hoops away from the corners is larger than that near the corners.
- The ultimate load carrying capacity of ASCC column was increased with the increase of concrete strength, steel ratio and confined core diameter, and the decrease of spiral pitch, batten spacing, diameter of hoops (with same volumetric ratio) and diameter of longitudinal bars (with same reinforcement ratio).
- The toughness of ASCC column showed an increase when the concrete strength, steel ratio increase, and the confined core diameter and diameter of longitudinal bar (with same reinforcement ratio) decrease. The spiral pitch, batten spacing and diameter of hoops (with same volumetric ratio) did not have a significant effect on the toughness.
- The ductility of the ASCC column increases as the steel ratio increases, and the concrete strength, spiral pitch, batten spacing, diameter of hoops (with same volumetric ratio), diameter of longitudinal bars (with same reinforcement ratio) and confined core diameter decrease.
- A calculation approach is proposed to predict the ultimate load carrying capacity of ASCC column under axial compression. Using the well-established confining concrete model proposed by Mander, the different behaviors of the unconfined and the confined concretes are calculated and the possibility of buckling of the steel angles is explicitly considered. The predicted results agree well with the results from experiment.

Acknowledgments

The research described in this paper was financially supported by the National Natural Science Foundation of China (51578163), the Natural Science Foundation of Guangxi (2016GXNSFDA380032), High Level Innovation Group and Outstanding Scholar Program Project of Guangxi High Education (No: [2017]38), and the Innovation Project of Guangxi Graduate Education (YCBZ2015009). The writers also appreciate the assistance that was provided by Chengui Jing and Qihong Tan during the experimental process.

References

- ACI 209R-92 (1997), Prediction of Creep, Shrinkage and Temperature Effects in Concrete Structures; American Concrete Institute, Farmington Hills, MI, USA.
- Adam, J.M., Ivorra, S., Pallarés, F.J., Giménez, E. and Calderón, P.A. (2009), "Axially loaded RC columns strengthened by steel caging. Finite element modelling", *Constr. Build. Mater.*, **23**(6), 2265-2276.
- Campian, C., Nagy, Z. and Pop, M. (2015), "Behavior of fully encased steel-concrete composite columns subjected to monotonic and cyclic loading", *Procedia Engineering*, **117**, 439-451.
- Campione, G. (2011), "RC columns strengthened with steel angles and battens: experimental results and design procedure", *Practice Periodical on Structural Design and Construction*, **18**(1), 1-11.
- Campione, G. (2012), "Strength and ductility of RC columns strengthened with steel angles and battens", *Constr. Build. Mater.*, **35**, 800-807.
- Cavaleri, L., Trapani, F.D., Ferrotto, M.F. and Davi, L. (2017), "Stress-strain models for normal and high strength confined concrete: Test and comparison of literature models reliability in reproducing experimental results", *Ingegneria Sismica*, **34**(3-4), 114-137.
- Chinese Standard GB/T 50081-2002 (2002), Standard for test method of mechanical properties on ordinary concrete; China Ministry of Construction, Beijing, China. [In Chinese]
- Chinese Standard GB 50010-2010 (2010), Code for Design of Concrete Structures; China Ministry of Construction, Beijing, China. [In Chinese]
- Chinese Standard GB/T 700-2006 (2006), Carbon structural steels; China National Standardization Management Committee, Beijing, China. [In Chinese]
- Chinese Standard GB 50017-2014 (2014), Code for Design of Steel Structures; China Ministry of Construction, Beijing, China. [In Chinese]
- Ding, F.X., Fang, C., Bai, Y. and Gong, Y.Z. (2014), "Mechanical performance of stirrup-confined concrete-filled steel tubular stub columns under axial loading", *J. Constr. Steel Res.*, **98**, 146-157.
- Eom, T.S., Hwang, H.J., Park, H.G., Lee, C.N. and Kim, H.S. (2013), "Flexural test for steel-concrete composite members using prefabricated steel angles", *J. Struct. Eng.*, **140**(4), 04013094.
- Frangou, M., Pilakoutas, K. and Dritsos, S. (1995), "Structural repair/strengthening of RC columns", *Constr. Build. Mater.*, **9**(5), 259-266.
- Garzón-Roca, J., Adam, J.M. and Calderón, P.A. (2011), "Behaviour of RC columns strengthened by steel caging under combined bending and axial loads", *Constr. Build. Mater.*, **25**(5), 2402-2412.
- Hwang, H.J., Eom, T.S., Park, H.G. and Lee, S.H. (2016), "Axial Load and Cyclic Lateral Load Tests for Composite Columns with Steel Angles", *J. Struct. Eng.*, **142**(5), 04016001.
- Kim, C.S., Park, H.G., Chung, K.S. and Choi, I.R. (2013), "Eccentric axial load capacity of high-strength steel-concrete composite columns of various sectional shapes", *J. Struct. Eng.*, **140**(4), 04013091.
- Ky, V.S., Tangaramvong, S. and Thepchatri, T. (2015), "Inelastic analysis for the post-collapse behavior of concrete encased steel composite columns under axial compression", *Steel Compos. Struct., Int. J.*, **19**(5), 1237-1258.
- Mander, J.B., Priestley, M.J. and Park, R. (1988), "Theoretical stress-strain model for confined concrete", *J. Struct. Eng.*, **114**(8), 1804-1826.
- Montuori, R. and Piluso, V. (2009), "Reinforced concrete columns strengthened with angles and battens subjected to eccentric load", *Eng. Struct.*, **31**(2), 539-550.
- Nagaprasad, P., Sahoo, D.R. and Rai, D.C. (2009), "Seismic strengthening of RC columns using external steel cage", *Earthq. Eng. Struct. Dyn.*, **38**(14), 1563-1586.
- Sheikh, S.A. and Uzumeri, S.M. (1980), "Strength and ductility of tied concrete columns", *J. Struct. Div.*, **106**(ASCE 15388 Proceeding).

- Shih, T.H., Chen, C.C., Weng, C.C., Yin, S.Y.L. and Wang, J.C. (2013), "Axial strength and ductility of square composite columns with two interlocking spirals", *J. Constr. Steel Res.*, **90**, 184-192.
- Somes, N.F. (1970), "Compression Tests on Hoop-Reinforced Concrete", *J. Struct. Div.*, **96**(7), 1495-1509.
- Wang, K., Yuan, S.F., Cao, D.F. and Zheng, W.Z. (2015), "Experimental and numerical investigation on frame structure composed of steel reinforced concrete beam and angle-steel concrete column under dynamic loading", *Int. J. Civil Eng.*, **13**(2A), 137-147.
- Wu, Y.F., Liu, T. and Oehlers, D.J. (2006), "Fundamental principles that govern retrofitting of reinforced concrete columns by steel and FRP jacketing", *Adv. Struct. Eng.*, **9**(4), 507-533.
- Xiao, C., Deng, F., Chen, T. and Zhao, Z. (2017), "Experimental study on concrete-encased composite columns with separate steel sections", *Steel Compos. Struct., Int. J.*, **23**(4), 483-491.
- Yang, F., Sun, L., Zhao, J., Wu, D. and Li, W. (2015), "Behavior of a novel circular HSC column with double high strength spirals", *Adv. Struct. Eng.*, **18**(9), 1371-1382.
- Zheng, W. and Ji, J. (2008), "Dynamic performance of angle-steel concrete columns under low cyclic loading-I: Experimental study", *Earthq. Eng. Eng. Vib.*, **7**(1), 67-75.